http://dx.doi.org/10.1109/JPHOTOV.2012.2200455

Analysis of Phosphorus Doped Silicon Oxide Layers Deposited by Means of PECVD as a Dopant Source in Diffusion Processes

A. Fallisch, D. Wagenmann, R. Keding, D. Trogus, M. Hofmann, J. Rentsch, H. Reinecke, D. Biro

***Abstract*— In order to increase the conversion efficiencies of silicon solar cells, advanced cell structures with selectively doped areas receive an increasing interest. There is a strong need to separate the contacted diffusion profiles from the non-contacted. On the one hand, a high dopant concentration in the contact regime reduces the series resistance losses mainly due to lowered contact resistance. Additionally recombination is reduced by shielding the minority charge carriers from surface at the contact. On the other hand a low dopant concentration in the non-contact regime reduces the recombination losses and optimizes the spectral response of the cell.**

In this work phosphorus doped silicon oxide layers are used as a diffusion source for tube furnace diffusion processes. It is shown that the sheet resistance of the diffused area is controlled by the silane gas flow during the deposition of phosphorus doped silicon oxide. In order to analyze the influence of the diffused areas on the saturation current densities, symmetrical carrier lifetime samples are prepared. Therefore a stack system consisting of a thermally grown silicon dioxide and silicon nitride is used for passivation purposes on textured samples.

***Index Terms*—PECVD, doped oxide, sheet resistance, diffusion**

I. Introduction

INCREASING the solar cell efficiency while keeping the costs constant is one way to reduce the costs per Watt-peak in crystalline silicon solar cells. The emitter is a highly doped region which collects excess minority charge carriers from the bulk. Since the emitter is usually situated at the front side of the solar cell it is mainly responsible for the height of the short-circuit current density J_{sc} in the short wavelength range extracted from the device. Passivated solar cells like the "passivated emitter and rear cell" (PERC) [1] or the "passivated emitter and rear locally diffused cell" (PERL) [2] receive an increasing interest because they yield a higher efficiency potential. As these cells are no longer limited by the recombination rate at the full area back surface field (BSF), the necessity of low emitter recombination is given to further increase the efficiency. A low emitter recombination is achieved by reducing the dopant concentration, especially at the surface [3]. Minority charge carriers generated in the highly doped emitter region have to diffuse to the pn-junction before they recombine. Thus a shallow emitter is also important to increase the short-circuit current density as about 10% of the maximum achievable current is generated in the first few hundred nanometers [4]. This is in contrast to the need of a high surface concentration and a deep emitter in the contact region. A high surface concentration reduces the contact resistance [5] and a deep emitter shields minority charge carriers from the highly recombinative surface [6] and reduces the shunting probability due to the metallization.

Furthermore cell concepts like the emitter wrap-through (EWT) [7] or back-junction back-contact (BC-BJ) [8, 9] cell concept, which feature an interdigitated grid need a n^+-p^+ pattern on the rear side. Such a doping pattern can be achieved e.g. by multiple diffusion steps in interaction with diffusion barriers as in [10], by laser doping [11] or laser chemical processes [12].

Another possibility is to use a doped silicon oxide layer as a diffusion source as shown in [13]. Such a layer can be used, as already demonstrated earlier in [14-16], in a co-diffusion process or to replace phosphorus oxychloride ($POCl_3$) as in [17]. Doped silicon nitride layers may also be used as a replacement for $POCl_3$ as shown in [18]. In this work phosphorus doped silicon oxide layers, also denoted as phosphosilicate glass (PSG) are deposited by means of plasma-enhanced chemical vapor deposition (PECVD) on the sample surfaces before the diffusion process. Such layers can also be patterned with inkjet technology as recently shown by Keding et al. [19]. In the following it is shown that these PSG layers can be used in several diffusion processes with different thermal budgets leading to phosphorus doped areas with varying dopant concentration profiles.

II. Experimental

In the first experiments the influence of the silane gas flow on the sheet resistance R_{sh} is analysed for a specific diffusion process at a plateau temperature of 850°C. For this purpose Czochralski (Cz) grown boron-doped silicon wafers with a

Manuscript received March 16, 2012; revised April 18, 2012; accepted May 7, 2012; Date of publication June 14, 2012.

A. Fallisch, D. Wagenmann, R. Keding, D. Trogus, M. Hofmann, J. Rentsch and D. Biro are with the Fraunhofer Institute for Solar Energy Systems ISE, Freiburg, Germany. Corresponding Author: Arne Fallisch, phone: +49 761 4588 5046; e-mail: arne.fallisch@ise.fraunhofer.de.

H. Reinecke is with the Institute for Microsystems Engineering, University of Freiburg, Freiburg, Germany.

http://dx.doi.org/10.1109/JPHOTOV.2012.2200455

resistivity of ρ = 1-3 Ωcm are used. The process flow is depicted on the left hand side of Fig. 1. After the saw damage removal and a subsequent cleaning step one side is coated with a PECVD silicon oxide layer (SiO_x) which acts as a diffusion barrier. On the other side different PSG layers of more than 100 nm thickness are deposited. These are capped with an undoped silicon oxide layer of approximately 153 nm thickness as a diffusion barrier and to avoid a chemical reaction of the PSG with the ambience in the subsequent tube furnace process. Silane (SiH_4) and nitrous oxide (N_2O) are used as reactant gases to deposit the silicon oxide. Trimethyl phosphite (TMPi, $P(OCH_3)_3$) is additionally let into the process chamber for doping with argon (Ar) as a carrier gas. The temperature of the bubbler containing the TMPi is kept constant below room temperature. The amount of phosphorus in the deposited sheet is dependent on the silane Ψ_{SiH4} and the argon $\Psi_{Ar\ (TMPi)}$ gas flow during the deposition process and thus influences the sheet resistance R_{sh} of the emitter after diffusion. In this work these gas flows are varied while all other parameters are kept constant. After the deposition process the samples are diffused in a tube furnace. The sheet resistance is measured using an inductive inline measurement setup [20]. These samples are denoted as *Resistance-samples*. The results are presented in the next section.

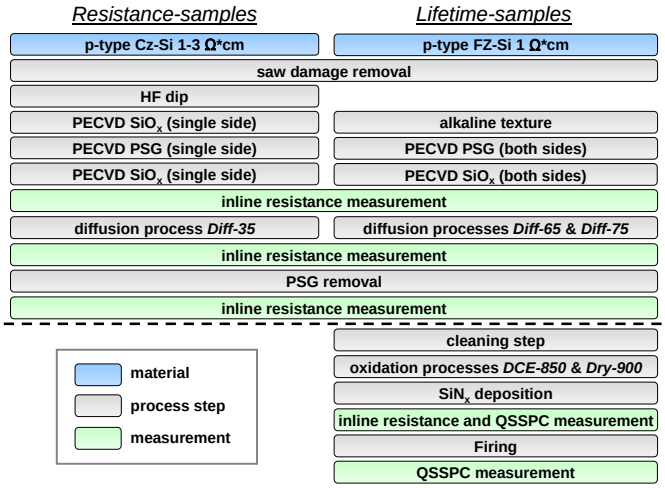

Fig. 1: Process flow for the fabrication of phosphorus doped samples to evaluate the sheet resistance R_{sh} using an inline measurement equipment [20] and the lifetime using quasi steady-state photoconductance measurements [21, 22].

For the second experiment a similar process sequence has been chosen as depicted on the right hand side of Fig. 1. As this experiment is also designed to determine the emitter saturation current density J_{0e}, float zone (FZ) silicon material with a resistivity of ρ = 1 Ωcm is used since it provides reliably high bulk lifetimes. In this case the samples represent the front side of a solar cell and are therefore textured in an alkaline solution. The PSG layer is deposited on both sides to achieve symmetrically processed lifetime samples. The PSG layers are capped with a PECVD silicon oxide. After the diffusion in the tube furnace the PSG layer is removed in a wet chemical bath containing hydrofluoric acid. These samples are denoted as *Lifetime-samples*. The results concerning the sheet resistances measured after diffusion are presented in the next section.

The samples finally receive a short oxidation process with a subsequent silicon nitride (SiN_x) deposition for passivation and optical confinement. Afterwards a firing process is applied and the effective minority carrier lifetime is measured with the quasi-steady-state photoconductance method (QSSPC) [21, 22]. The results concerning the emitter saturation current densities are discussed in section V.

III. Emitter Sheet Resistance

A. Process parameters

The first thermal process which is used to process the planar *Resistance-samples* features a peak temperature of 850°C. This process is denoted as *Diff-35*. The silane gas flow for the deposition of the PSG layer is varied between 15 and 45 sccm depending on the Ar (TMPi) gas flow which is either 5 or 10 sccm.

Table 1: Denomination of the applied PECVD, thermal and oxidation processes with their specific process parameters: silane and Ar (TMPi) gas flows Ψ_{SiH4} and $\Psi_{Ar\ (TMPi)}$, diffusion and oxidation plateau temperatures T_{diff} and T_{ox}.

PECVD process	Ψ_{SiH4} **[sccm]**	$\Psi_{Ar\ (TMPi)}$ **[sccm]**
PECVD-15-5	15	5
PECVD-20-5	20	5
PECVD-25-5	25	5
PECVD-30-5	30	5
PECVD-35-5	35	5
PECVD-25-10	25	10
PECVD-30-10	30	10
PECVD-35-10	35	10
PECVD-37-10	37	10
PECVD-40-10	40	10
PECVD-45-10	45	10

thermal process	T_{diff} **[°C]**
Diff-35	850
Diff-65	820
Diff-75	820

oxidation process	T_{ox} **[°C]**
DCE-850	850
Dry-900	900

The textured *Lifetime-samples* receive two different thermal processes at a peak temperature of 820°C. The first of these thermal processes is denoted as *Diff-65* and the second is denoted as *Diff-75*. The silane gas flow used for the deposition of the PSG layer is varied between 30 and 45 sccm, whereas the Ar (TMPi) gas flow is kept constant at $\Psi_{Ar\ (TMPi)}$ = 10 sccm. The given oxidation processes *DCE-850* and *Dry-900* are used for passivation of the lifetime samples. Both oxidation processes have a short oxidation time at peak temperature. The *DCE-850* oxidation is performed at 850°C in a dichloroethylene (DCE) environment. The oxidation *Dry-900* has a peak temperature of 900°C and is performed in a oxygen environment. An overview over the denomination of all processes with their specific parameters is given in Table 1.

If $POCl_3$ is used as a phosphorus diffusion source during the tube furnace process *Diff-35*, an emitter sheet resistance of

http://dx.doi.org/10.1109/JPHOTOV.2012.2200455

approximately 35 Ω/sq is achieved. This process is denoted as *$POCl_3$-35* process. The thermal processes *Diff-65* and *Diff-75* result in sheet resistances of 65 and 75 Ω/sq using $POCl_3$ and are denoted as *$POCl_3$-65* and *$POCl_3$-75*.

B. *Sheet resistance in dependence on silane gas flow*

In the following the $POCl_3$ diffusion source is replaced by a PECVD deposited doped oxide and the sheet resistance R_{sh} of the diffused samples is analysed. Fig. 2 depicts the dependence of the sheet resistance on silane gas flow using different Ar (TMPi) gas flows and diffusion processes. The lowest sheet resistance of R_{sh} = 30 Ω/sq is measured on samples featuring deposition process *PECVD-15-5* with subsequent thermal process *Diff-35*. Thus a deviation in the sheet resistance of 5 Ω/sq is present compared to the same thermal process using $POCl_3$ for doping. In the $POCl_3$ diffusion, gas is introduced into the furnace after the peak temperature of 850°C is reached. If a PECVD PSG layer is used as a diffusion source, phosphorus already diffuses into the silicon during the heating period to reach the diffusion temperature. For an increasing silane gas flow the concentration of phosphorus, let into the chamber by Ar, is diluted. Thus the sheet resistance increases exponentially up to R_{sh} = 72 Ω/sq (*PECVD-35-5 + Diff-35*). Increasing the amount of Ar (TMPi) from 5 to 10 sccm shifts all data points to the right as is depicted in Fig. 2 for samples diffused in the thermal process *Diff-35*. Decreasing the thermal budget during diffusion, as in *Diff-65* and *Diff-75*, shifts the curve upwards to higher sheet resistances R_{sh}. The exponential behaviour is independent of the varied parameters in the investigated parameter range.

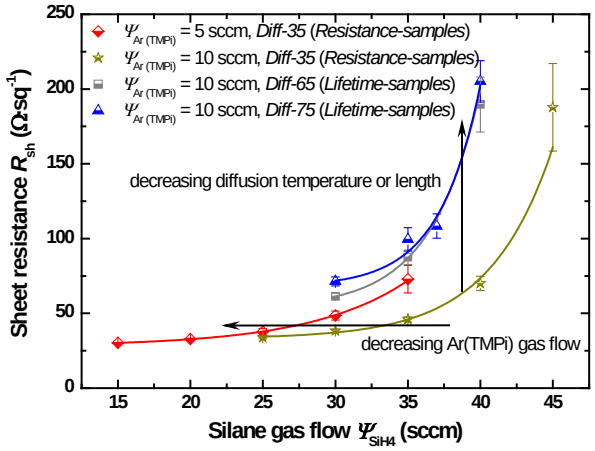

Fig. 2: Impact of the silane gas flow Ψ_{SiH4} on the sheet resistance R_{sh} for different Ar (TMPi) gas flows $\Psi_{Si\ (TMPi)}$. The sheet resistance is measured with an inline equipment [20] after diffusion. A higher Ar (TMPi) gas flow shifts the curve to the right, whereas a diffusion at a lower temperature and/or shorter diffusion dwell time shifts the curve upwards to higher sheet resistances R_{sh}. The lines shall guide the eye.

For increasing silane gas flows, the sheet resistance tends to get inhomogeneous as becomes evident regarding the standard deviation in Fig. 2. At a silane gas flow of Ψ_{SiH4} = 45 sccm the inline measured sheet resistance varies between 150 and 213 Ω/sq (*Diff-35 + PECVD-45-10*).

During PECVD four samples lie next to each other orthogonal to the movement direction of the carrier. The inductive inline measurement is done at three different positions on a single wafer, which are likewise orthogonal to the carrier movement direction as shown at the top of Fig. 3. This allows a space-resolved examination of the sheet resistance R_{sh} in x-direction which is depicted at the bottom of Fig. 3 using an Ar (TMPi) gas flow of $\Psi_{Ar\ (TMPi)}$ = 10 sccm during deposition and a *Diff-35* thermal process for the diffusion. For low silane gas flows up to 40 sccm the sheet resistance is quite homogeneous. The standard deviation of the sheet resistance is approximately 4.8 Ω/sq. Above silane gas flows of 40 sccm the inhomogeneity of the sheet resistance increases excessively. Using a silane gas flow of Ψ_{SiH4} = 45 sccm results in standard deviation of 29.3 Ω/sq. For diffusion process at lower temperatures the inhomogeneity is higher for the same silane gas flows due to the sensitivity of the sheet resistance on the phosphorus doping. Thus the usable silane gas flow parameter range is also dependent on the applied thermal process.

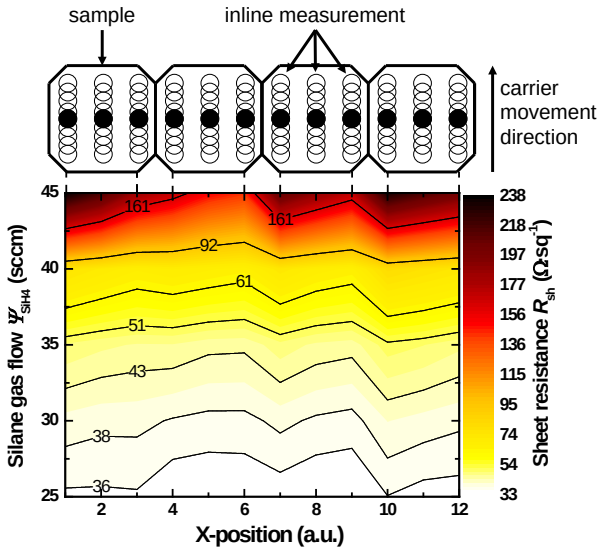

Fig. 3: Sheet resistance measured after diffusion in dependence of the silane gas flow and the position on the PECVD carrier orthogonal to the carrier movement direction. Every three positions belong to one sample. The horizontal lines represent constant sheet resistance values.

These results reveal that the sheet resistance is controllable by the silane and Ar (TMPi) gas flows. Emitter with sheet resistances up to 100 Ω/sq can be diffused quite homogeneous. In the following section the phosphorus doping profiles diffused from PSG layers are analysed and the effect of subsequent oxidation process on the profiles is discussed.

IV. PHOSPHORUS PROFILES

A. *Phosphorus profiles after diffusion*

To measure the phosphorus doping profiles in silicon after diffusion shiny etched samples are processed. These receive a short etching step in hydrofluoric acid to remove native silicon

http://dx.doi.org/10.1109/JPHOTOV.2012.2200455

oxide before the PSG deposition. After diffusion the PSG layers are removed in hydrofluoric acid. Phosphorus is diffused from three different deposited PSG layers with silane gas flows of 30, 35 and 40 sccm. For the diffusion the thermal process *Diff-75* is used. Some samples are measured after the PSG removal with secondary ion mass spectrometry (SIMS). For the remaining samples the oxidation process *DCE-850* is applied to investigate the dependence of a subsequent high temperature step, needed for passivation, on the doping profiles.

The phosphorus profiles measured after the PSG removal are depicted in Fig. 4. A *POCl$_3$-75* diffused emitter is shown as a reference. Regarding the diffused doping profiles reveals that the total phosphorus concentration as well as the emitter depth is reduced for increasing silane gas flow during the PSG deposition. Due to a measurement artefact in the first few nanometers, the exact surface concentration cannot be determined. Nevertheless, to receive a surface concentration N_s an exponential extrapolation of the phosphorus profile in the first few nanometers is applied. The emitter depth d_e is defined at a doping concentration of $N_D = 1 \cdot 10^{17}$ cm^{-3}, due to great scattering of the measurement data at low doping densities.

The dash-dotted line in Fig. 4 at a phosphorus concentration of $2.6 \cdot 10^{20}$ cm^{-3} marks the equilibrium concentration n_{eq} according to Solmi et al. [23]. This equilibrium concentration is dependent on the peak temperature of the last high temperature step, which in this case is the diffusion temperature of 820°C. Regions in silicon with phosphorus concentrations exceeding the equilibrium concentration contain electrically inactive phosphorus. The inactive phosphorus can be mobile and immobile which is dependent on the saturation concentration C_{sat} [23]. Above the saturation concentration phosphorus exists as immobile SiP precipitates [23, 24]. These reduce the lifetime and consequently lead to higher saturation current densities [25]. All diffused emitters still have a fraction of electrically inactive phosphorus which partly also exceeds the saturation concentration of $C_{sat} = 3.4 \cdot 10^{20}$ cm^{-3}.

If a silane gas flow of $\Psi_{SiH4} = 30$ sccm is used during the deposition of the PSG the emitter is slightly deeper ($d_e = 383$ nm) compared to an emitter diffused from $POCl_3$ ($d_e = 327$ nm). This is due to enhanced diffusion time for the PSG as already mentioned in the previous section. The surface concentration is with $1.3 \cdot 10^{21}$ cm^{-3} slightly higher ($N_s = 7.7 \cdot 10^{20}$ cm^{-3} for *POCl$_3$-75*). The emitter with the highest silane gas flow of $\Psi_{SiH4} = 40$ sccm has the lowest surface concentration of $N_s = 7.6 \cdot 10^{20}$ cm^{-3} and slightest depth of $d_e = 315$ nm.

The indicated sheet resistance values are determined by integration of the phosphorus profile. For the calculation the incomplete ionization of the phosphorus according to Schenk et al. [26], the equilibrium concentration n_{eq} and the mobility model according to Klassen [27, 28] is taken into account. The values calculated from the phosphorus profiles are in correlation with the inline measured values, which are shown in brackets in Fig. 4. The highest sheet resistance of $R_{sh} = 121$ Ω/sq is achieved on samples diffused from PSG layer featuring the highest silane gas flow of $\Psi_{SiH4} = 40$ sccm during deposition.

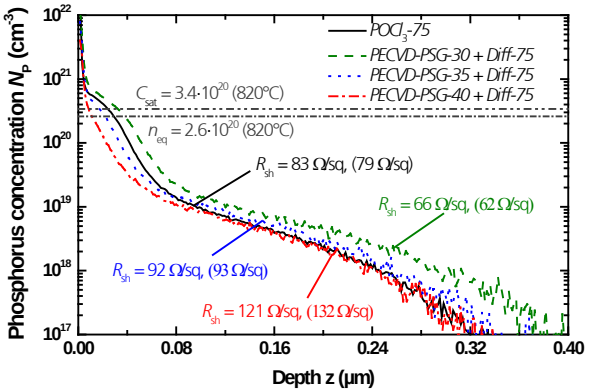

Fig. 4: Phosphorus doping profiles diffused from three different PECVD-PSG layers using a *Diff-75* diffusion process. A *POCl$_3$-75* diffused emitter is shown as a reference. Secondary ion mass spectrometry is used to measure the phosphorus concentration. For each profile the calculated and inline measured, shown in brackets, sheet resistance R_{sh} of the emitter is given. The horizontal lines mark the equilibrium concentration n_{eq} and the saturation concentration C_{sat} of phosphorus at 820°C according to Solmi et al. [23].

These results prove that a higher silane gas flows during the PSG deposition leads to a decreasing surface concentration and emitter depth and an increment of the sheet resistance.

B. Phosphorus profiles after oxidation

To further decrease the surface concentration and to achieve a high passivation quality at the surface some samples are oxidized. As is depicted in Fig. 5 the *DCE-850* oxidation process reduces the surface concentration and drives in the emitter. The cleaning process prior to the oxidation removes a few nanometres of highly doped silicon [29] increasing the sheet resistance. Whether this effect is compensated by the subsequent oxidation is dependent on the diffused emitter profile and the oxidation process.

The equilibrium concentration n_{eq} is increased to $2.8 \cdot 10^{20}$ cm^{-3} due to the higher temperature of the oxidation process compared to the diffusion process. Thus electrically inactive phosphorus near the surface becomes electrically active. The sheet resistance of the emitter diffused from $POCl_3$ is reduced from 83 after diffusion to 78 Ω/sq after the DCE oxidation. The surface concentration is reduced to $2.1 \cdot 10^{20}$ cm^{-3} whereas the emitter depth is increased to 510 nm. The emitter diffused from PSG layers deposited using the process *PECVD-30* is only slightly changed regarding the sheet resistance which is around 70 Ω/sq after the oxidation. The surface concentration is reduced down to $2.1 \cdot 10^{20}$ cm^{-3} and the emitter depth is enhanced to 566 nm. For a higher silane gas flow of 35 sccm (*PECVD-35*) during the PSG deposition the sheet resistance is increased from 92 to 141 Ω/sq. As the width of the highly doped region (kink part of the profile) for this emitter is narrower before the oxidation compared to a *PECVD-30* diffused emitter, the influence of

http://dx.doi.org/10.1109/JPHOTOV.2012.2200455

the cleaning step on the sheet resistance is much higher. The surface concentration is with $6.5 \cdot 10^{19}$ cm^{-3} far below the equilibrium concentration of $n_{eq} = 2.8 \cdot 10^{20}$ cm^{-3}. The emitter depth is 413 nm.

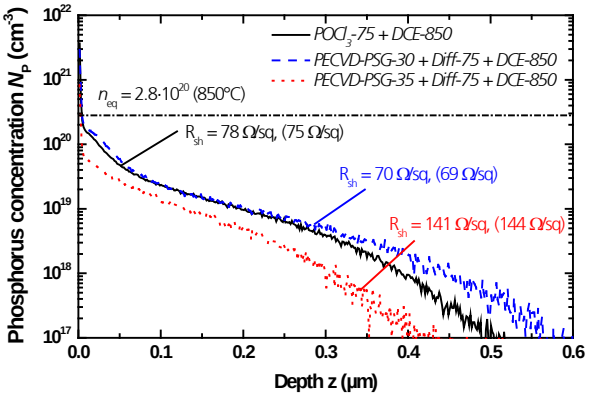

Fig. 5: Phosphorus profiles diffused from three different PECVD-PSG layers deposited by means of PECVD using a thermal process *Diff-75* with a subsequent *DCE-850* oxidation. A *POCl$_3$-75* diffused and oxidized emitter is shown as a reference. Secondary ion mass spectrometry is used to measure the phosphorus concentration. For each profile the calculated and inline measured, shown in brackets, sheet resistance R_{sh} of the emitter is given. The dashed-dotted horizontal line marks the equilibrium concentration n_{eq} of phosphorus at 850°C according to Solmi et al. [23].

The diffusion profiles predict a reduced Auger recombination for increasing silane gas flows. As the surface areas are passivated a reduced surface recombination is expected. For all diffused emitter the extracted surface concentration is below the equilibrium concentration after the oxidation process. To evaluate the recombination properties of the discussed emitters, the saturation current densities are determined in the next section.

V. Emitter Saturation Current Density

Symmetric lifetime samples, which contain the discussed emitters diffused from PECVD PSG, have been analyzed regarding their emitter saturation current densities J_{0e}. The emitter saturation current density is determined by the low injection method as for example described in [30]. Thus the emitter saturation current density is described by

$$J_{0e} = \frac{q n_i^2}{S_{eff}\left(N_A + \Delta n\right)}$$

where $q = 1.602 \cdot 10^{-19}$ C is the elementary charge of an electron, $n_i = 9.16 \cdot 10^9$ cm^{-3} is the intrinsic carrier concentration at room temperature ($T = 25$°C), S_{eff} is the effective surface recombination velocity, $N_A = 1.48 \cdot 10^{16}$ is the bulk doping concentration and $\Delta n = 1 \cdot 10^{15}$ cm^{-3} is the excess carrier concentration. The effective surface recombination for symmetrical processed samples is given by [31]

$$S_{eff} = \frac{W}{2\left[\left(\frac{1}{\tau_{eff}} - \frac{1}{\tau_b}\right)^{-1} - \frac{W^2}{D\pi^2}\right]}$$

where W is the sample thickness, τ_{eff} is the effective minority carrier lifetime, τ_b is the intrinsic bulk lifetime and $D = 27.09$ cm^2/s is the diffusion coefficient. The instrinsic bulk lifetime is only limited by the Auger and radiative recombination which is calculated as shown in [32], yielding ~3 ms for 1 Ωcm silicon wafers as used in this work.

All lifetime samples have a surface with random pyramids and are approximately 163 µm thick. The amount of phosphorus in PSG is adjusted by varying the silane gas flow (*PECVD-30-10*, *35-10* and *37-10*). Half of the samples are diffused using the thermal process *Diff-65* and the other half using *Diff-75*. For passivation purposes the samples receive two different oxidation processes: *DCE-850* and *Dry-900*. For nearly all oxidized samples the SiO_2 thickness is about 10-15 nm. All samples diffused with *PECVD-30-10* and *35-10* layer as a diffusion source and combined with *DCE-850* oxidation exhibit an SiO_2 thickness > 25 nm.

Subsequently a silicon nitride is deposited on top of the SiO_2 (cf. Fig. 1). To realize a front side as it would be processed in a real solar cell device, the thickness of the subsequently deposited silicon nitride is adapted to yield a low reflectance. On the samples with an oxide thickness > 25 nm a silicon nitride of approximately 43 nm thickness is deposited, whereas on the other samples a silicon nitride of 56 nm thickness is deposited on both sides. Afterwards the emitter saturation current densities are determined and shown in Fig. 6 on the left hand side. The strong dependence of sheet resistance on the emitter saturation current density is clearly visible and expected. For increasing sheet resistances the saturation current densities decrease. The lowest saturation current densities around $J_{0e} = 100$ fA/cm^2 are reached using the *PECVD-37-10* process for the PSG deposition, combined with thermal process *Diff-75* and the oxidation process *DCE-850*. The sheet resistance of around 160 Ω/sq for this process sequence is very high. Such layers could be used for the diffusion of a front surface field [33, 34] in back-contact back-junction solar cells.

Using a low silane gas flow as in *PECVD-30-10*, a diffusion with the longest dwell time as in *Diff-65* and an oxidation at a temperature of 900°C as in *Dry-900* results in sheet resistances of $R_{sh} < 40$ Ω/sq. These emitters feature the highest emitter saturation current densities above 300 fA/cm^2. All other J_{0e}-values lie between 100 and 300 fA/cm^2. If $POCl_3$ is used as a diffusion source (number 0 next to the data points in Fig. 6) the saturation current densities are around 350 fA/cm^2 for a sheet resistance around 52 Ω/sq.

The lifetime samples are fired in an industrial firing oven to see whether the passivation system is temperature stable. During the firing process the hydrogen within the silicon nitride diffuses to the Si/SiO_2 interface and further reduces the

http://dx.doi.org/10.1109/JPHOTOV.2012.2200455

recombination by saturating dangling bonds [35, 36]. The emitter saturation current densities measured after the firing process are depicted in Fig. 6 on the right hand side.

While the emitter saturation current density of some samples that received the *Dry-900* oxidation process is decreased after the firing step, the J_{0e}-values of the samples with *DCE-850* oxidation stay approximately on the same level. This is the case for all samples that received the deposition *PECVD-30-10* and *35-10*. The emitter saturation current densities of the samples with *PECVD-30-10*, *Diff-65* and *Dry-900* are reduced from over 300 to below 270 fA/cm^2. Although the sheet resistance of these samples ($R_{sh} \approx 38$ Ω/sq) is lower compared to the samples which received a *DCE-850* oxidation ($R_{sh} \approx 58$ Ω/sq), the emitter saturation current density is lower. This is possibly due to a lower surface concentration which can be expected due to the higher thermal budget of the *Dry-900* oxidation process. However, the slightly thicker SiN_x and the thinner SiO_2 layer on these samples might also affect the reduction of the J_{0e}-values after firing. The $POCl_3$ diffused samples exhibit a reduction in J_{0e} due to firing below 300 fA/cm^2 but the J_{0e}-values are still higher compared to the J_{0e}-values achieved using a *PECVD-30-10* diffusion source.

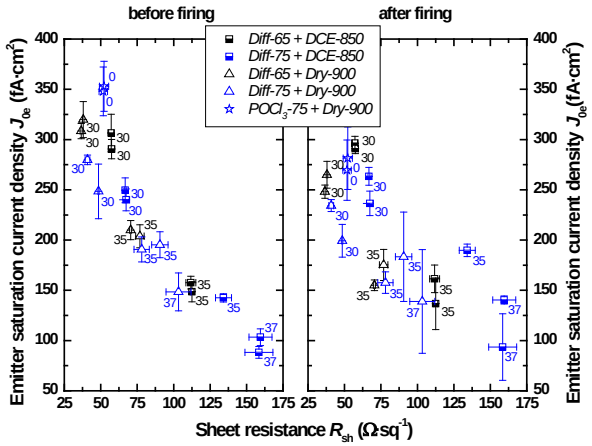

Fig. 6: Emitter saturation current densities J_{0e} of SiO_2/SiN_x passivated samples before and after firing depending on the emitter resistivity R_{sh} for two diffusion processes (*Diff-65* and *Diff-75*) and two different oxidation processes (*DCE-850* and *Dry-900*). The error bars mark the standard deviation. The sheet resistance is dependent on the silane gas flow (0, 30, 35 or 37 sccm) during the PECVD-PSG deposition process (number next to data points). The number 0 marks a $POCl_3$ diffused reference.

On samples that received a PSG deposition process *PECVD-37-10* the emitter saturation current density is in some cases increased and in others decreased. No clear tendency is attributed to firing. The lowest emitter saturation current densities around 100 fA/cm^2 are found again for sheet resistances in the range of 160 Ω/sq. For sheet resistance between 100 and 120 Ω/sq the saturation current densities are around 150 fA/cm^2 which enables maximum open-circuit voltages of $V_{oc} = 675$ mV. Such layers could be used for a selective emitter approach in solar cells featuring front contacts or in EWT solar cells.

VI. Conclusion

A comprehensive analysis of PECVD PSG layers as alternative diffusion sources has been shown. The amount of phosphorus in the PSG layer is controlled by the silane gas flow during the PECVD. Therefore the sheet resistance as well as the surface concentration and the emitter depth are also dependent on the silane gas flow. A higher silane gas flow during the PSG deposition leads to a decreased surface concentration and emitter depth and an increased sheet resistance.

The achieved results in terms of sheet resistances are highly reproducible, especially for low silane gas flows $\Psi_{SiH4} < 30$ sccm and constant argon flow $\Psi_{Ar\ (TMPi)} = 10$ sccm during deposition of PSG. The deviation in the sheet resistance is on the same level as for $POCl_3$ diffusion processes. Thus PSG layers can be used as an alternative diffusion source in industrial diffusion processes. To achieve a higher throughput for the PECVD machine, the belt velocity can be increased which results in a reduced thickness of the PSG layers. In earlier publications a 50 nm thick PSG layer has been still sufficient as an infinite doping source [37]. When the same applies for the process used in this work, the belt velocity could be doubled, leading to a higher throughput. The PSG layers can also be used in combination with inline diffusion process.

Using higher silane gas flows of $\Psi_{SiH4} \geq 35$ sccm leads to reduced phosphorus surface concentrations. Such layers are also attractive for the usage in co-diffusion processes, avoiding a second high temperature step. For very high silane gas flows of $\Psi_{SiH4} \geq 45$ sccm during deposition, corresponding to high sheet resistances above 200 Ω/sq, the process still has to be improved in terms of homogeneity to achieve an industrial applicability.

A high passivation quality on the phosphorus-doped area diffused from PSG layers is achieved using a double layer antireflection coating consisting of a thermally grown silicon dioxide and a silicon nitride. The oxidation process reduces the surface concentration below the equilibrium concentration. Emitter saturation current densities around 150 fA/cm^2 are achieved for sheet resistances between 100 and 120 Ω/sq. Such processes can for example be used in a co-diffusion process to create a selective emitter pattern on the front side of PERC or PERL cells or to improve the blue response in EWT solar cells. For higher sheet resistance around 150 Ω/sq, saturation current densties of $J_{0e} = 100$ fA/cm^2 are possible which can be used for the diffusion of a front surface field as used in back-contact back-junction solar cells.

Acknowledgment

The authors would like to thank all PV-TEC co-workers and specifically R. Neubauer for sample preparation and J. Benick for fruitful discussions.

http://dx.doi.org/10.1109/JPHOTOV.2012.2200455

REFERENCES

[1] A. W. Blakers, A. Wang, A. M. Milne, J. Zhao and M. A. Green, "22.8% efficient silicon solar cell", *Applied Physics Letters*, **vol**. **55**, 1989, pp. 1363-1365.

[2] J. Zhao, A. Wang and M. A. Green, "24% efficient PERL structure silicon solar cells", in Proc. *21st IEEE PVSC*, Kissimmee, Florida, USA, 1990, pp. 333-335.

[3] R. R. King, R. A. Sinton and R. M. Swanson, "Studies of diffused phosphorus emitters: saturation current, surface recombination velocity, and quantum efficiency", *IEEE Transactions on Electron Devices*, **vol**. **37**, 1990, pp. 365-371.

[4] M. A. Green and M. J. Keevers, "Optical properties of intrinsic silicon at 300 K", *Progress in Photovoltaics: Research and Applications*, **vol**. **3**, 1995, pp. 189-192.

[5] D. K. Schroder and D. L. Meier, "Solar cell contact resistance - a review", *IEEE Transactions on Electron Devices*, **vol**. **ED-31**, 1984, pp. 637-647.

[6] A. Goetzberger, B. Voss and J. Knoblauch, "Sonnenenergie: Photovoltaik", Stuttgart: Teubner Verlag, 1997.

[7] J. M. Gee, W. K. Schubert and P. A. Basore, "Emitter wrap-through solar cell", in Proc. *23rd IEEE PVSC*, Louisville, Kentucky, USA, 1993, pp. 265-270.

[8] M. D. Lammert and R. J. Schwartz, "The interdigitated back contact solar cell: a silicon solar cell for use in concentrated sunlight", *IEEE Transactions on Electron Devices*, **vol**. **ED-24**, 1977, pp. 337-342.

[9] R. J. Schwartz and M. D. Lammert, "Silicon solar cells for high concentration applications", in Proc. *Technical Digest of the International Electron Devices Meeting*, Washington, DC, 1975, pp. 350-352.

[10] R. Woehl, M. Rüdiger, D. Erath, D. Stüwe, R. Preu and D. Biro, "Structuring technology and simulation of high efficiency back-contact back-junction silicon solar cells under low concentration", in Proc. *AIP Conference*, Freiburg, Germany, 2010, pp. 53-57.

[11] U. Jäger, M. Okanovic, M. Hörteis, A. Grohe and R. Preu, "Selective emitter by laser doping from phosphosilicate glass", in Proc. *24th EU PVSEC*, Hamburg, Germany, 2009, pp. 1740-1743.

[12] D. Kray, N. Bay, G. Cimiotti, S. Kleinschmidt, N. Kösterke, A. Lösel, M. Sailer, A. Träger, H. Kühnlein, H. Nussbaumer, C. Fleischmann and F. Granek, "Industrial LCP selective emitter solar cells with plated contacts", in Proc. *35th IEEE PVSC*, Honolulu, Hawaii USA, 2010, pp. 667-671.

[13] J. Benick, J. Rentsch, C. Schetter, C. Voyer, D. Biro and R. Preu, "PECVD PSG as a dopant source for industrial solar cells", in Proc. *21st EU PVSEC*, Dresden, Germany, 2006, pp. 1012-1015.

[14] A. Fallisch, D. Stüwe, R. Neubauer, D. Wagenmann, R. Keding, J. Nekarda, R. Preu and D. Biro, "Inkjet structured EWT silicon solar cells with evaporated aluminum metallization and laser-fired contacts", in Proc. *35th IEEE PVSC*, Honolulu, Hawaii, USA, 2010, pp. pp. 6.

[15] N. Mingirulli, D. Stüwe, J. Specht, A. Fallisch and D. Biro, "Screen-printed emitter-wrap-through solar cell with single step side selective emitter with 18.8% efficiency", *Progress in Photovoltaics: Research and Applications*, **vol**. **19**, 2011, pp. 366-374.

[16] N. Mingirulli, D. Stüwe, J. Specht, R. Keding, R. Neubauer, A. Fallisch and D. Biro, "18.8% EWT-cells with screen-printed metallization and single step side selective emitter formation", in Proc. *24th EUPVSEC*, Hamburg, Germany, 2009, pp. 1979-1984.

[17] D. Trogus, J. Seiffe, F. Pillath, M. Hofmann, A. Wolf and J. Rentsch, "Phosphoric anti-reflective coatings as dopant source and front-side passivation for industrial silicon solar cell manufactoring", in Proc. *26th EU PVSEC*, Hamburg, Germany, 2011, pp. 1361-1364.

[18] B. Paviet-Salomon, S. Manuel, S. Gall, R. Monna, A. Slaoui, L. Vandroux, R. Hida and S. Dechenaux, "Selective emitter silicon solar cells without $POCl_3$ Furnace Diffusion", in Proc. *26th EU PVSEC*, Hamburg, Germany, 2011, pp. 1369-1371.

[19] R. Keding, R. Woehl, D. Stüwe, A. Fallisch, M. Hofmann, J. Rentsch and D. Biro, "Diffusion and characterization of doped patterns in silicon from prepatterned boron- and phosphorus-doped silicate glasses ", in Proc. *26th EU PVSEC*, Hamburg, Germany, 2011, pp. 1385-1389.

[20] M. Spitz, U. Belledin and S. Rein, "Fast inductive inline measurement of the emitter sheet resistance in industrial solar cell fabrication", in Proc. *22nd EUPVSEC*, Milan, Italy, 2007, pp. 47-50.

[21] R. A. Sinton and A. Cuevas, "Contactless determination of current-voltage characteristics and minority-carrier lifetimes in semiconductors from quasi-steady-state photoconductance data", *Applied Physics Letters*, **vol**. **69**, 1996, pp. 2510-2512.

[22] R. A. Sinton, A. Cuevas and M. Stuckings, "Quasi-steady-state photoconductance, a new method for solar cell material and device characterization", in Proc. *25th IEEE PVSC*, Washington DC, USA, 1996, pp. 457-460.

[23] S. Solmi, A. Parisini, R. Angelucci, A. Armigliato, D. Nobili and L. Moro, "Dopant and carrier concentration in Si in equilibrium with monoclinic SiP precipitates", *Physical Review B*, **vol**. **53**, 1996, pp. 7836-7841.

[24] M. Finetti, P. Negrini, S. Solmi and D. Nobili, "Electrical properties and stability of supersaturated phosphorus-doped silicon layers", *Journal of the Electrochemical Society: Solid-State Science and Technology*, **vol**. **128**, 1981, pp. 1313-1317.

[25] P. Ostoja, S. Guerri, P. Negrini and S. Solmi, "The effects of phosphorus precipitation on the open-circuit voltage in N+/P silicon solar cells", *Solar Cells*, **vol**. **11**, 1984, pp. 1-12.

[26] A. Schenk, P. P. Altermatt and B. Schmithusen, "Physical model of incomplete ionization for silicon device simulation", in Proc. *11th SISPAD*, Monterey, USA, 2006, pp. 51-54.

[27] D. B. M. Klaassen, "A unified mobility model for device simulation - I. Model equations and concentration dependence", *Solid State Electronics*, **vol**. **35**, 1992, pp. 953-959.

[28] D. B. M. Klaassen, "A unified mobility model for device simulation - II. Temperature dependence of carrier mobility and lifetime. " *Solid State Electronics*, **vol**. **35**, 1992, pp. 961-967.

[29] A. Kimmerle, A. Wolf, U. Belledin and D. Biro, "Modelling carrier recombination in highly phosphorus-doped industrial emitters", *Energy Procedia*, **vol**. **8**, 2011, pp. 275-281.

[30] C. Reichel, F. Granek, J. Benick, O. Schultz-Wittmann and S. W. Glunz, "Comparison of emitter saturation current densities determined by quasi-steady-state photoconductance measurements of effective carrier lifetimes at high and low injections", in Proc. *23rd EU PVSEC*, Valencia, Spain, 2008, pp. 1664-1669.

[31] A. B. Sproul, "Dimensionless solution of the equation describing the effect of surface recombination on carrier decay in semiconductors", *Journal of Applied Physics*, **vol**. **76**, 1994, pp. 2851-2854.

[32] M. J. Kerr and A. Cuevas, "General parameterization of Auger recombination in crystalline silicon", *Journal of Applied Physics*, **vol**. **91**, 2002, pp. 2473-2480.

[33] F. Granek, M. Hermle, C. Reichel, A. Grohe, O. Schultz-Wittmann and S. Glunz, "Positive effects of front surface field in high-efficiency back-contact back-junction n-type silicon solar cells", in Proc. *33rd IEEE PVSC*, San Diego, USA, 2008, pp. 1-5.

[34] F. Granek, C. Reichel, M. Hermle, D. M. Huljic, O. Schultz and S. W. Glunz, "Front surface passivation of n-type high-efficiency back-junction silicon solar cells using front surface field", in Proc. *22nd EU PVSEC*, Milan, Italy, 2007, pp. 1454-1457.

[35] C. Boehme and G. Lucovsky, "Dissociation reactions of hydrogen in remote plasma-enhanced chemical-vapor-deposited silicon nitride", *J. Vac. Sci. Technol. A*, **vol**. **19**, 2001, pp. 2622.

[36] H. F. W. Dekkers, L. Carnel and G. Beaucarne, "Carrier trap passivation in multicrystalline Si solar cells by hydrogen from SiN_x:H layers", *Applied Physics Letters*, **vol**. **89**, 2006, pp. 1-3.

[37] Mingirulli, "Fabrication and characterization of emitter-wrap-through cells", Ph.D. dissertation, *Department of Physics*, University of Konstanz, 2009, pp. 144.